Fusion Engineering and Design 171 (2021) 112516

Contents lists available at ScienceDirect

Fusion Engineering and Design

journal homepage: www.elsevier.com/locate/fusengdes

Assessment of the burning-plasma operational space in ITER by using a control-oriented core-SOL-divertor model

Vincent Graber *, Eugenio Schuster

Mechanical Engineering and Mechanics, Lehigh University, Bethlehem, PA 18015, USA

ARTICLE INFO

Keywords:
ITER
Scrape-off layer
Divertor
Burn control
Plasma operations

ABSTRACT

In future tokamaks, the control of burning plasmas will require careful regulation of the plasma density and temperature. Along with the design of effective burn-control systems, understanding how the fusion power varies in the density-temperature space is vital for the operation of fusion power plants. In this work, the steady-state operational space of ITER is studied using a control-oriented core-plasma model coupled to a two-point model of the scrape-off-layer (SOL) and divertor regions. The two models are coupled through the exchange of input-output parameters. The deuterium and tritium recycling from the wall are output parameters of the SOL-divertor model that are used as input parameters in the core-plasma density balance. Furthermore, the separatrix temperature, which is an output parameter of the SOL-divertor model, is incorporated into the radial core-plasma temperature profiles. Therefore, the temperature-dependent power balance of the plasma core is intimately linked to the SOL-divertor model. Both the power entering the SOL from the core, as determined by the core-plasma power balance, and the separatrix density, as dictated by the core-plasma density balance, are input parameters to the SOL-divertor model. They are control knobs in the SOL-divertor model that can be regulated using the core-plasma actuators: auxiliary power and pellet injection. There are various operational limitations, such as the saturation of the aforementioned actuators, that will prevent ITER from accessing certain high-fusion plasma regimes. The achievable tritium concentration in the fueling lines and the maximum sustainable heat load on the divertor will impose further restrictions. By accounting for these limitations, the ITER operational space is computed based on the coupled core-SOL-divertor model and visualized using Plasma Operation Contour (POPCON) plots that map performance metrics, such as the fusion to auxiliary power ratio, over the density-temperature space. Comparisons are drawn between plasmas with different recycling, confinement, and SOL-divertor conditions.

1. Introduction

The safe operation of burning plasmas in ITER will require real-time regulation of the core-plasma's density and temperature along with the conditions in the plasma's edge. The sensitivity of the plasma core to the conditions in the scrape-off-layer (SOL) and divertor regions (and vice versa) makes achieving burn control and divertor objectives more challenging. For example, increasing the fusion power (burn control objective) could risk the melting of plasma-facing components by increasing the heat flow crossing the separatrix and intensifying the heat load deposited on the divertor plate. In this work, a core-SOL-divertor model that couples zero-dimensional differential equations for the particle and energy densities within the separatrix with a two-point model of the plasma's edge is presented. In the core-plasma, deuterium and tritium particles are burned up in fusion events that produce alpha particles. The temperatures of the ions and electrons in the core are assumed to have radial profiles that are parabolically shaped and include the temperature at the separatrix (specifically at an upstream position). Since the upstream separatrix temperature is determined by the two-point model, the core-plasma power balance is directly dependent on SOL-divertor conditions. The SOL-divertor conditions also determine the strength of the wall-recycling that helps fuel the plasma's core. In kind, the core-plasma's total density and power have a strong influence on the SOL-divertor plasma. Since the core's density and power are readily modulated with the use of actuators (primarily pellet injection and neutral beam injection), they behave as control knobs for the plasma's edge.

Actuator constraints will prevent ITER from accessing certain

* Corresponding author.
E-mail address: graber@lehigh.edu (V. Graber).

https://doi.org/10.1016/j.fusengdes.2021.112516
Received 30 November 2020; Received in revised form 15 March 2021; Accepted 18 March 2021
Available online 16 April 2021

desirable plasma regimes that have a high fusion power. Between the electron cyclotron, ion cyclotron and neutral beam heating systems, ITER will have a total of 73 MW of auxiliary power available [1]. Deuterium (D) and tritium (T) in the core will be refueled with a D injector that fires 100% D pellets and a deuterium-tritium (DT) injector that fires 10%D-90%T pellets [2]. The D injector and the DT injector will have a maximum throughput of 120 Pa m^3/s and 111 Pa m^3/s, respectively. During long pulses, the T concentration in the DT pellets may fall below the 90% nominal value. Because of this, ITER's accessibility to adequate T refueling is a concern. Actuator constraints are not the only restrictions to the ITER plasma system. The heat load on the divertor target must be limited to a maximum of 10 MW/m^2 to avoid catastrophic melting. Finally, the H-mode confinement regime and divertor detachment should be maintained.

In this work, all of the aforementioned constraints are mapped to Plasma Operation Contour (POPCON) plots that span over density-temperature space. The region in these POPCON plots that meets all of the constraints gives the set of achievable plasma regimes in ITER for a certain set of plasma conditions. In a previous work [3], the authors performed POPCON analysis based on core-specific constraints (e.g. the maximum deuterium and tritium pellet injection rate) and the zero-dimensional differential equations of the core-plasma's density and energy. This work advances this prior analysis with a coupled core-edge model that allows the consideration of edge-specific constraints (e.g. the maximum divertor target heat load) and the core-plasma's dependency on edge-plasma conditions. The POPCON analysis in this work reveals the sensitivity of the ITER operable space to the conditions and constraints in the edge-plasma.

This paper is organized as follows. In Section 2, the model of the plasma's core is presented. The two-point model of the plasma's edge that is coupled with the core-plasma model is given in Section 3. In Section 4, POPCON analysis is used to study operational constraints in ITER. Finally, conclusions are drawn and possible future work is considered in Section 5.

2. The core-plasma model

The model of the plasma's core is bounded by the separatrix, and it is derived from one-dimensional rate equations for the ion and energy densities. To match expectations for ITER, the radial temperature and density profiles are assumed to be parabolic and flat, respectively [4]. The radial temperature profiles have the shape:

$$T_i(t,\psi) = (T_{i,0} - T_u)(1 - \psi/\psi_0)^2 + T_u, \tag{1}$$

$$T_e(t,\psi) = (T_{e,0} - T_u)(1 - \psi/\psi_0)^2 + T_u, \tag{2}$$

where $T_{i,0}$ and $T_{e,0}$ are, respectively, the peaked ion and electron central temperatures of the core-plasma, T_u is the plasma temperature at the separatrix, ψ is the toroidal magnetic flux coordinate, and ψ_0 is the total flux enclosed at the separatrix [5]. With the assumption of flat particle density profiles, the plasma core's total density (ions and electrons) is simply $n(t,\psi) = n(t) = n_u$ where n_u is the density at the separatrix.

By taking the volume average of the one-dimensional equations, the zero-dimensional model of the core can be found to be

$$\frac{d}{dt}n_D = -\frac{n_D}{\tau_D} - S_\alpha + f_s S_D^{rec} + S_D, \tag{3}$$

$$\frac{d}{dt}n_T = -\frac{n_T}{\tau_T} - S_\alpha + f_s S_T^{rec} + S_T, \tag{4}$$

$$\frac{d}{dt}n_\alpha = -\frac{n_\alpha}{\tau_\alpha} + (1 - f_{loss})S_\alpha, \tag{5}$$

$$\frac{d}{dt}E_i = -\frac{E_i}{\tau_{E,i}} + f_i P_\alpha + P_{ei} + P_{aux,i}, \tag{6}$$

$$\frac{d}{dt}E_e = -\frac{E_e}{\tau_{E,e}} + f_e P_\alpha - P_{ei} - P_{br} + P_{ohm} + P_{aux,e}, \tag{7}$$

where n_D, n_T and n_α are the deuterium (D), tritium (T) and alpha-particle ion densities, S_α is the fusion reaction rate density, f_{loss} is the fraction of alpha particles that are lost before they deposit all of their kinetic energy into the plasma because of MHD events, S_D^{rec} and S_T^{rec} are the D and T recycling sources (given in Section 3), $f_s \ll 1$ is the shielding factor [6], S_D and S_T are the external fueling rates from pellet injection, and $P_{aux,i}$ and $P_{aux,e}$ are the auxiliary powers delivered to the ions and electrons. The total auxiliary power from the external electron cyclotron, ion cyclotron and neutral beam heating systems is $P_{aux} = P_{aux,i} + P_{aux,e}$. The temperature-dependent ion and electron energy densities are given by

$$E_i = \frac{3}{2}(n_D + n_T + n_\alpha + n_I)\left\langle T_i \right\rangle, \tag{8}$$

$$E_e = \frac{3}{2}n_e\left\langle T_e \right\rangle = \frac{3}{2}(n_D + n_T + 2n_\alpha + Z_I n_I)\left\langle T_e \right\rangle, \tag{9}$$

where n_I with atomic number Z_I is the impurity particle density and the electron density n_e is determined from the quasi-neutrality condition. For brevity, the volume average of the ion and electron temperatures is denoted using $\langle T_i \rangle$ and $\langle T_e \rangle$ instead of writing it explicitly in terms of $T_{i,0}$, $T_{e,0}$ and T_u. The bremsstrahlung radiation losses, the ohmic heating [7], and the collisional ion-electron power exchange [8] are given by

$$P_{br} = 5.5 \times 10^{-37} Z_{eff} n_e^2 \left\langle T_e^{1/2} \right\rangle, \tag{10}$$

$$P_{ohm} = 2.8 \times 10^{-9} Z_{eff} I_p^2 a^{-4} \left\langle T_e^{-3/2} \right\rangle, \tag{11}$$

$$P_{ei} = \frac{3}{2}n_e \frac{\langle T_e \rangle - \langle T_i \rangle}{\tau_{ei}}, \tag{12}$$

where $I_p = 15$ MA and $a = 2$ m are the plasma current and minor radius for ITER, respectively, and T_e is expected in keV in (10) and (11). The effective atomic number and the energy relaxation time are, respectively,

$$Z_{eff} = \frac{n_D + n_T + 4n_\alpha + Z_I^2 n_I}{n_e}, \tag{13}$$

$$\tau_{ei} = \frac{3\pi\sqrt{2\pi}\varepsilon_0^2 \left\langle T_e^{3/2} \right\rangle}{e^4 m_e^{1/2} ln\Lambda} \sum_{ions} \frac{m_i}{n_i Z_i^2}, \tag{14}$$

where $e = 1.622 \times 10^{-19}$C, $m_e = 9.1096 \times 10^{-31}$kg, $\varepsilon_0 = 8.854 \times 10^{-12}$F/m and $ln\Lambda \approx 17$ [7].

As seen from (12) and (14), an estimate is used for the volume average of P_{ei} in (6) and (7) because finding a closed-form solution was not tractable. The impact of taking this approach, which is similar to that taken in [9], is negligible because P_{ei} does not appear in the plasma power balance (16). Therefore, it does not influence the energy confinement time (τ_E), the total auxiliary power or the SOL-divertor model presented in Section 3. Exact closed-form solutions were used for volume averages of the remaining power terms (P_α, P_{br} and P_{ohm}) in (6) and (7).

The alpha-particle power $P_\alpha = f_{loss} Q_\alpha S_\alpha$, where $Q_\alpha = 3.52$MeV, is proportional to S_α. The DT reactivity [10], which determines $S_\alpha = n_D n_T \langle \sigma\nu \rangle$, is given by

$$\begin{aligned} \langle \sigma\nu \rangle &= G(T_{i,0}) \times C_1 \omega \sqrt{\xi \Big/ (m_r c^2 T_{i,0}^3)} e^{-3\xi}, \\ \omega &= T_{i,0}\left[1 - \frac{T_{i,0}(C_2 + T_{i,0}(C_4 + T_{i,0}C_6))}{1 + T_{i,0}(C_3 + T_{i,0}(C_5 + T_{i,0}C_7))}\right]^{-1}, \end{aligned} \tag{15}$$

where $\xi = (B_G^2/4\omega)^{1/3}$, B_G, $m_r c^2$ and C_j for $j \in \{1, \ldots, 7\}$ are constants.

The correction factor $G(T_{i,0})$ is used to account for the volume-averaging procedure [9]. Using the model found in [11], approximately $f_e \approx 80\%$ and $f_i \approx 20\%$ of the alpha-particle power, P_α, are delivered, respectively, to the plasma electrons and ions in ITER.

The IPB98(y,2) scaling law for the global energy confinement time of H-mode plasmas [12] is

$$\begin{aligned} \tau_E &= 0.0562 H I_p^{0.93} R^{1.97} B^{0.15} M^{0.19} \varepsilon^{0.58} \kappa^{0.78} n_e^{0.41} P_{tot}^{-0.69}, \\ P_{tot} &= (P_\alpha + P_{aux} - P_{br} + P_{ohm}) \times V, \end{aligned} \tag{16}$$

where P_{tot} is the total plasma power in MW, $V = 840$ m^3 is the plasma volume, H is the enhancement factor, B is the toroidal magnetic field, $R = 6.2$ m is the plasma major radius, $\kappa = 1.7$ is the vertical elongation at the 95% flux surface, $\varepsilon = a/R$, $M = 3\gamma + 2(1-\gamma)$, $\gamma = n_T/(n_D + n_T)$, and n_e has units of 10^{19} m^{-3} (values are for ITER). The confinement times in (3)–(7) are assumed to be proportional to τ_E such that $\tau_D = k_D \tau_E$, $\tau_T = k_T \tau_E$, $\tau_\alpha = k_\alpha \tau_E$, $\tau_{E,i} = k_i \tau_E$ and $\tau_{E,e} = k_e \tau_E$ where k_D, k_T, k_α, k_i and k_e are constants.

When the total plasma power (16) exceeds a certain power threshold (P_{thresh}), the plasma is considered to be in H-mode. When $P_{tot} < P_{thresh}$, the plasma is in L-mode. The threshold power for the L-H mode transition is

$$P_{thresh} = 4.3 M^{-1} B^{0.772} n_e^{0.782} R^{0.999} a^{0.975}, \tag{17}$$

where P_{thresh} is in MW [13]. Maintaining H-mode operation is considered a constraint of the system because the IPB98(y,2) scaling law for τ_E was generated from a database of H-mode plasmas from various tokamaks.

The two external fueling rates, S_D and S_T, are supplied by two pellet injectors that fire pellets into guide tubes that lead to the plasma. The D pellet injector fuels the plasma at a rate of S_D^{line} using 100% D pellets (tritium concentration of $\gamma_D^{line} = 0$). The DT pellet injector supplies D and T to the plasma at a total rate of S_{DT}^{line}. The nominal tritium concentration of DT pellets is $\gamma_{\mathrm{DT}}^{line} = 90\%$, but it may fall below 90% during long pulses. The relationship between the total rates of D and T externally injected into the core (S_D and S_T) and the output of the two pellet injectors (S_D^{line} and S_{DT}^{line}) is

$$S_D = C_{eff}[(1-\gamma_{\mathrm{DT}}^{line}) S_{\mathrm{DT}}^{line} + (1-\gamma_D^{line}) S_D^{line}], \tag{18}$$

$$S_T = C_{eff}[\gamma_{\mathrm{DT}}^{line} S_{\mathrm{DT}}^{line} + \gamma_D^{line} S_D^{line}], \tag{19}$$

where C_{eff} is the pellet mass loss factor. For ITER, pellets are expected to lose approximately 10% ($C_{eff} = 90\%$) of their mass while traveling along the guide tubes [2]. Pellet fueling loses efficiency as the temperature of the plasma edge increases. This could eventually be modeled by making C_{eff} inversely proportional to a function of T_u.

3. The SOL-divertor plasma model

The two-point model relates upstream separatrix conditions at the outer-midplane to downstream separatrix conditions at the divertor target. It is defined by assuming particle, pressure and power balances along the SOL:

$$2 n_t T_t = f_{mom} n_u T_u, \tag{20}$$

$$T_u^{7/2} = T_t^{7/2} + \frac{7}{2} \frac{f_{cond} q_\parallel L}{\kappa_0}, \tag{21}$$

$$(1 - f_{pow}) q_\parallel = \gamma_s n_t T_t c_{\mathrm{st}}, \tag{22}$$

where n_u and T_u are the upstream density and temperature, n_t and T_t are the downstream density and temperature, $q_\parallel$ is the parallel power flux density, $\kappa_0 = 2000$ is the parallel conductivity coefficient, L is the connection length which is defined as half of the along-field distance between the two divertor plates, $\gamma_s = 7$ is the sheath heat transmission coefficient, and c_{st} is the plasma sound speed. Correction factors for conduction (f_{cond}), momentum losses (f_{mom}) and power losses (f_{pow}) are included [6].

Below, the two-point model given by (20)–(22) is rewritten in terms of two readily regulated core-plasma quantities: the upstream density n_u [m^{-3}] and the power entering the SOL from the core P_{SOL} [W]. This is done in part by assuming that P_{SOL} enters the SOL entirely via perpendicular conduction, relating the power scrape-off width $\lambda_{q\parallel}$ to n_u and P_{SOL}, and replacing $q_\parallel$ with P_{SOL} in the two-point model (20)–(22). The power entering the SOL is defined by the total plasma power (16) such that $P_{SOL} = P_{tot}$. With radial density profiles that are flat, $n_u = n_D + n_T + n_\alpha + n_I + n_e$. Because of the two-point model's sensitivity to n_u and P_{SOL}, SOL conditions can be manipulated through the external heating and fueling of the core (P_{aux}, S_D and S_T).

The upstream and downstream temperatures in eV are

$$T_u = \left(\left(\frac{7^2}{8^2 \pi^3} \right) \frac{f_{cond} P_{SOL}^2 L}{e n_u \chi_\perp^{SOL} \kappa_0 a R^2 (B_\theta/B)_u} \right)^{\frac{2}{9}}, \tag{23}$$

$$\begin{aligned} T_t &= 2.67 \times 10^{-3} \left(\frac{(1-f_{pow})^2}{f_{mom}^2 f_{cond}^{\frac{8}{9}}} \right) \left(\frac{m_i}{\gamma_s^2 e^{\frac{37}{9}}} \right) \\ &\quad \times \frac{P_{SOL}^{\frac{20}{9}} \kappa_0^{\frac{8}{9}}}{n_u^{\frac{28}{9}} (\chi_\perp^{SOL})^{\frac{10}{9}} L^{\frac{8}{9}} (B_\theta/B)_u^{\frac{10}{9}} a^{\frac{10}{9}} R^{\frac{20}{9}}}, \end{aligned} \tag{24}$$

where $\chi_\perp^{SOL}$ is the anomalous cross-field heat thermal diffusivity, $(B_\theta/B)_x$ is the ratio of the poloidal field over the total field at the upstream ($x = u$) or downstream ($x = t$) location, and m_i is the average ion mass. For ITER, $L = 75$ m, $\chi_\perp^{SOL} = 1$ m^2 s^{-1}, $(B_\theta/B)_u = 0.3$ and $(B_\theta/B)_t = 0.075$ are expected [6,14,15].

The power flux density (W/m^2) deposited on the target, which must be kept low enough to avoid catastrophic melting, is given by

$$\begin{aligned} q_{dep} &= 1.61 \times 10^{-2} (cos\beta) (f_{cond})^{-\frac{2}{9}} \frac{(B_\theta/B)_t}{(B_\theta/B)_u} \\ &\quad \times \left(\frac{P_{SOL}^2}{e n_u \chi_\perp^{SOL}} \right)^{\frac{7}{9}} \left(\frac{\kappa_0^{\frac{2}{9}} (B_\theta/B)_u^{\frac{2}{9}}}{L^{\frac{2}{9}} R^{\frac{14}{9}} a^{\frac{7}{9}}} \right), \end{aligned} \tag{25}$$

where $cos\beta$ is included to account for target tilting. The effective angle β and the angle between the target's surface and the connecting field lines are complementary angles.

In this work, plasma-facing surfaces are assumed to be hydrogen saturated to match expectations for long pulse reactors like ITER [6]. The wall-recycling sources S_D^{rec} and S_T^{rec} in (3) and (4) are proportional to the particle flux density (m^{-2}s^{-1}) onto the divertor targets:

$$\begin{aligned} \Gamma_t &= \frac{7^{1/3} \pi}{2} \left(\frac{f_{mom}^2 f_{cond}^{2/3}}{(1-f_{pow})} \right) \left(\frac{\gamma_s e^{7/3}}{m_i} \right) \\ &\quad \times \left(\frac{n_u^7 L^2 a R^2 \chi_\perp^{\mathrm{SOL}} (B_\theta/B)_u}{P_{SOL}^2 \kappa_0^2} \right)^{1/3}. \end{aligned} \tag{26}$$

The recycling sources can then be found to be

$$S_D^{rec} = \left(\frac{n_D}{n_u} \right) \times \Gamma_t \frac{(B_\theta/B)_t A_{wet}}{V}, \tag{27}$$

$$S_T^{rec} = \left(\frac{n_T}{n_u} \right) \times \Gamma_t \frac{(B_\theta/B)_t A_{wet}}{V}, \tag{28}$$

where the plasma wetted area is given by

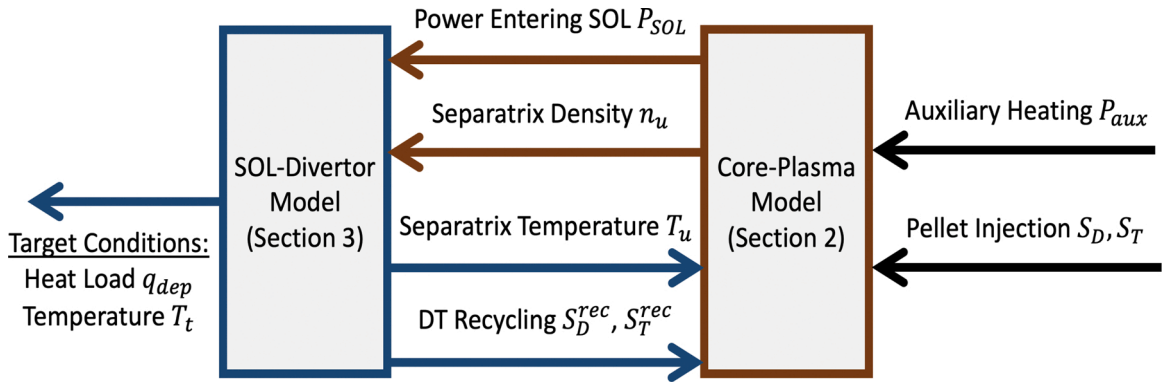

Fig. 1. Inputs and outputs of the core-plasma model (Section 2) and the SOL-divertor model (Section 3).

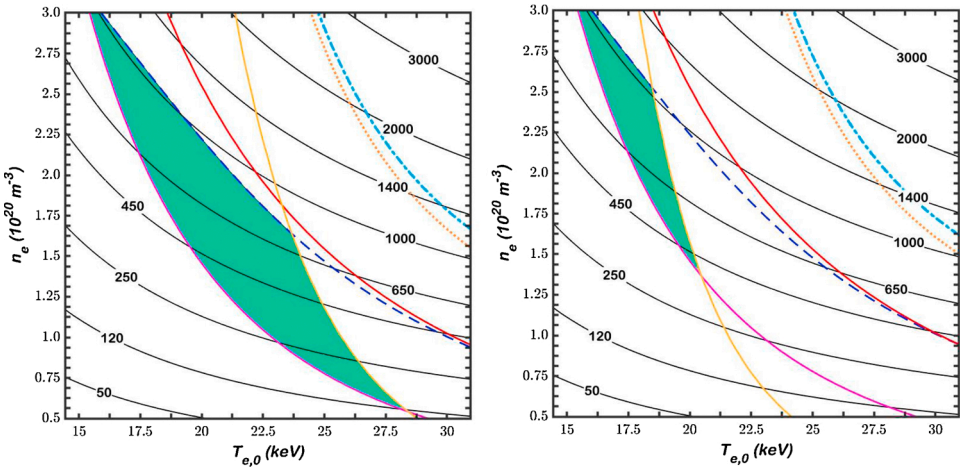

Fig. 2. On the left, the represented plasma has favorable SOL conditions: $f_{cond} = 1$, $f_{mom} = 0.3$, and $f_{pow} = 0.8$. On the right, the represented plasma has unfavorable SOL conditions: $f_{cond} = 0.9$, $f_{mom} = 0.5$, and $f_{pow} = 0.4$. Both plasmas consider target tilting ($\beta = 85°$). The black contour lines give the fusion power in MW. Each colored contour line represents a constraint of the plasma system: auxiliary power at 73 MW (blue-dashed line), DT injector with 90% T at 111 Pa m^3/s (orange-dotted line), D injector with 100% D at 120 Pa m^3/s (light-blue-dotted line), H-mode threshold $P_{tot} \geq P_{thresh}$ (magenta-solid line), target heat load at 10 MW/m^2 (red-solid line), and detachment requirement $T_t < 7$ eV (yellow-solid line). The space in green meets all of the constraints. (For interpretation of the references to color in this figure legend, the reader is referred to the web version of this article.)

$$A_{wet} = 4\pi R\left(\frac{(B_\theta/B)_u}{(B_\theta/B)_t}\right)\lambda_{q\|}(cos\beta)^{-1}. \tag{29}$$

The power scrape-off length (or power decay length) is

$$\lambda_{q\|} = \left(f_{cond}^{2/9}\right)\frac{8^{5/9}\pi^{4/3}}{7^{5/9}}\left(en_u\chi_\perp^{SOL}\right)^{7/9}P_{SOL}^{-5/9}\kappa_0^{-2/9}L^{2/9} \times (B_\theta/B)_u^{-2/9}a^{7/9}R^{5/9}. \tag{30}$$

Similar to the requirement of H-mode operation, maintenance of divertor detachment is assumed to be a constraint for ITER. The transition from the attached regime to the detached regime is assumed to occur when T_t falls below ~ 7 eV [16]. At low enough T_t, processes that are characteristic of detachment, such as ion-neutral friction, become significant [6]. The two-point model has been shown to match TOKAM3X-EIRENE simulations of WEST when an appropriate set of correction factors is used [17]. In [17], $f_{cond} = 1$, $f_{mom} = 0.2$ and $f_{pow} = 0.5$ was used for the detached regime, and $f_{cond} = 1$, $f_{mom} = 0.8$ and $f_{pow} = 0.1$ was used for the attached regime.

As shown in Fig. 1, the core-plasma model and the SOL-divertor model are coupled through various input-output parameters. The core-plasma model passes the power entering the SOL (P_{SOL}) and the separatrix density (n_u) to the SOL-divertor model. The SOL-divertor model feeds back the separatrix temperature (T_u) and the particle recycling (S_D^{rec} and S_T^{rec}) to the core-plasma model. The SOL-divertor model also provides the heat load on the target (q_{dep}) and the target temperature (T_t). External actuators, such as the auxiliary heating (P_{aux}) and pellet injection (S_D, S_T), directly and indirectly influence the core and edge plasmas.

4. Analysis of POPCON results

The following Plasma Operation Contour (POPCON) analysis is a study on steady-state plasma conditions in ITER. The POPCON plots span $n_e - T_{e,0}$ space. Each point of the POPCON plots is generated by solving the five dynamic equations of the core (3)–(7) in steady state (d/dt=0) simultaneously with the two-point model (23)–(30) for predefined n_e and $T_{e,0}$ values. The relationship $T_{i,0} = 0.8T_{e,0}$ is imposed because the central electron temperature is expected to be approximately 20% higher than the central ion temperature in ITER plasmas [4].

In Fig. 2, the POPCON plots of two similar plasmas with differing SOL conditions are compared. Both plasmas assume that $Z_I = 10$, $n_I/n_e = 0.01$, $f_s = 0.01$, $f_{loss} = 0.25$, $H = 0.9$, $k_D = 0.7$, $k_T = 0.7$, $k_\alpha = 0.9$, $k_i = 1$, $k_e = 1$, and $\beta = 85°$. In Fig. 2, a plasma with favorable SOL conditions ($f_{cond} = 1$, $f_{mom} = 0.3$, and $f_{pow} = 0.8$) is shown on the left, while the plasma represented on the right has unfavorable SOL conditions ($f_{cond} = 0.9$, $f_{mom} = 0.5$, and $f_{pow} = 0.4$). The fusion power ($P_{fus} = 5 \times P_\alpha$) in MW is shown with black contour lines over density-temperature space. The following actuator constraints are plotted: auxiliary power at 73 MW (blue-dashed line), DT injector with 90% T at 111 Pa m^3/s (orange-dotted line), and D injector with 100% D at 120 Pa m^3/s (light-blue-dotted line). The H-mode confinement threshold ($P_{tot} \geq P_{thresh}$) is met above the magenta-solid line. The divertor heat load is less than 10 MW/m^2 below the red-solid line. Divertor detachment ($T_t < 7$ eV) is achieved on the left side of the yellow-solid line. The area in density-temperature space where all of these constraints are met simultaneously is colored in green. This is the space where ITER can safely operate even at fusion powers in excess of 700 MW. For both plasmas, the limiting constraints

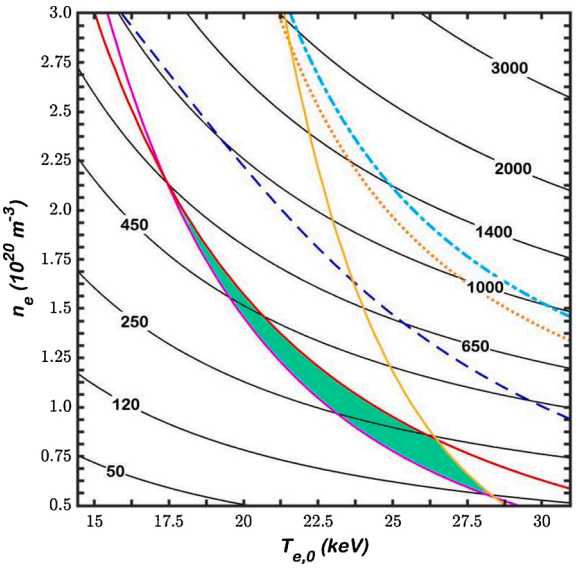

Fig. 3. The plasma represented in this figure has less target tilting ($\beta = 75°$) than the two plasmas represented in Fig. 2 ($\beta = 85°$). Since favorable SOL conditions ($f_{cond} = 1, f_{mom} = 0.3$ and $f_{pow} = 0.8$) are assumed, this figure should be compared to the plot on the left side of Fig. 2. See Section 4 for a full description of this figure.

that bound the green area are the H-mode confinement threshold, the maximum auxiliary heating of 73 MW, and the divertor detachment threshold. By comparing these two POPCON plots, it can clearly be seen that as the SOL conditions worsen the ITER operational space (the green area) shrinks.

The plasma represented in Fig. 3 has the same conditions as the plasma represented in the plot on the left side of Fig. 2 (favorable SOL conditions: $f_{cond} = 1$, $f_{mom} = 0.3$, and $f_{pow} = 0.8$) except that it has a lower β value. The value of β is 75° in Fig. 3 and 85° in Fig. 2. Recall that the $cos\beta$ term in (25) is used to account for the angle between the target's surface and the connecting magnetic field lines. A smaller β results in a magnification of the heat load on the target. As a result of this phenomenon, the maximum heat load of 10 MW/m^2 on the target (given by the red-solid line) restricts the ITER operable space in Fig. 3. In contrast, the operable regimes of the plasmas represented in Fig. 2 are restricted by the maximum auxiliary power instead of the maximum target heat load. With $\beta \approx 85°$ expected for ITER [15], the contrast between Fig. 2 and Fig. 3 demonstrates the importance of effective target tilting to avoid target melting during high-fusion operation.

5. Conclusions and future work

The POPCON analysis presented in this work shows that the achievable ITER operational space is very sensitive to conditions in the SOL. While the POPCON analysis shows that the requirement of divertor detachment drastically shrinks the ITER operable space when SOL conditions worsen (i.e. worse values for f_{cond}, f_{mom} and f_{pow}), in this study the constraint that prevents ITER from accessing higher fusion powers is either the maximum auxiliary power or the maximum target heat load. Even with unfavorable SOL conditions, ITER will eventually be capable of achieving fusion powers that exceed 700 MW as long as the degree of target tilting is sufficient. Sensitivity of the results to model assumptions is part of future work.

The POPCON plots, Fig. 2 and 3, suggest that the tritium concentration in ITER fueling lines is not the dominant constraint in this study. The tritium fueling is more than sufficient primarily because two other constraints, the maximum auxiliary power and the maximum target heat load, are considerably more restrictive than the maximum DT pellet injection rate. If different values for the model's parameters (e.g., $\chi_{\perp}^{SOL}$) were used when generating the POPCON data, then the maximum DT pellet injection rate and the tritium concentration could have been more relevant. A POPCON study that focuses on the impact of variations in the DT pellets' tritium concentration to ITER plasmas can be found in the authors' prior work [3].

To make the volume-averaging procedure for the differential equations tractable, simplified radial profiles for the temperatures and particle densities were assumed in this work. For future work, this volume-averaging procedure may be avoided. Instead, one-dimensional equations and profile shapes that include a pedestal could be employed. Furthermore, alternatives to the two-point model for the edge-plasma may be explored. In [18], SOLPS simulation results were used to develop parameterizations of edge-plasma conditions in terms of core-plasma conditions and external actuators. These simulations assumed a carbon-free tungsten divertor to match the plans for ITER. The one-dimensional equations of the core-plasma could be coupled with these SOLPS parameterizations to develop a more complex core-edge model. In addition, the inclusion of edge-plasma actuation, such as gas puffing and particle pumping, in a coupled core-edge model could be used to gain further insight into the ITER operational space.

Declaration of interests

None.

Declaration of Competing Interest

The authors report no declarations of interest.

Acknowledgments

This material is based upon work supported by the U.S. Department of Energy, Office of Science, Office of Fusion Energy under Award Number DE-SC-0010661.

References

[1] J.A. Snipes, et al., Actuator and diagnostic requirements of the ITER plasma control system, Fusion Eng. Des. 87(12).
[2] S.K. Combs, L.R. Baylor, et al., Overview of recent developments in pellet injection for ITER, Fusion Eng. Des. 87.
[3] V. Graber, E. Schuster, Tritium-Concentration Requirements in the Fueling Lines for High-Q Operation in ITER, European Physical Society, Milan, Italy, 2019.
[4] M. Shimada, et al., Physics design of ITER-FEAT, J. Plasma Fusion Res. 3 (2000) 77–83.
[5] R. Harvey, et al., Electron cyclotron heating and current drive in ITER, Nucl. Fusion 37(1).
[6] P. Stangeby, The Plasma Boundary, IOP, Bristol, 2000.
[7] J. Wesson, Tokamaks, 2nd ed., Clarendon Press, Oxford, 1997.
[8] R. Gross, Fusion Energy, Wiley-Interscience, New York, 1984.
[9] J.J. Martinell, J.E. Vitela, An optimal burn regime in a controlled tokamak fusion power plant, IEEE Trans. Plasma Sci. 44 (2016) 296–305.
[10] H.S. Bosch, G.M. Hale, Improved formulas for fusion cross-sections and thermal reactivities, Fusion Sci. Technol. 52(1).
[11] V. Graber, E. Schuster, Nonlinear adaptive burn control and optimal control allocation of over-actuated two-temperature plasmas, American Control Conference, Denver, USA (2020).
[12] M. Shimada, et al., Chapter 1: Overview and summary, Nucl. Fusion 47.
[13] Y.R. Martin, et al., Power requirement for accessing the h-mode in ITER, J. Phys. Conf. Ser. 123.
[14] C.S. Pitcher, P.C. Stangeby, Experimental divertor physics, Plasma Phys. Control. Fusion 39.
[15] R.A. Pitts, et al., Physics basis for the first ITER tungsten divertor, J. Nucl. Mater. Energy 20.
[16] J. Le, Z. Sizheng, Investigation of divertor detachment in east by two-point model, Plasma Sci. Technol. 9.
[17] Y.M.D. Fan, et al., Self-consistent coupling of the three-dimensional fluid turbulence code TOKAM3X and the kinetic neutrals code EIRENE, Contrib. Plasma Phys. 58.
[18] H.D. Pacher, et al., Impurity seeding in ITER DT plasmas in a carbon-free environment, J. Nucl. Mater. 463 (2015) 591–595.